Sulfide S and Pb Isotopic Constraint on the Genesis of Diyanqinamu Mo-Pb-Zn Polymetallic Deposit, Inner Mongolia, China

Hairui Sun [1,2,*], Zhilong Huang [2], Zhicheng Lü [1], Xiaofei Yu [1] and Yongsheng Li [1]

[1] Development Research Center of China Geological Survey, Beijing 100037, China; zhichenglv@163.com (Z.L.); xfyu@jlu.edu.cn (X.Y.); liysh1983@126.com (Y.L.)

[2] Stake Key Laboratory of Ore Deposit Geochemistry, Institute of Geochemistry, Chinese Academy Sciences, Guiyang 550081, China; huangzhilong@vip.gyig.ac.cn

[*] Correspondence: hairuisun@126.com; Tel.: +86-010-6206-1790

Abstract: The Great Hinggan Range (GHR) hosts many large Mo deposits and vein-type Pb-Zn deposits and is one of the most important polymetallic metallogenic belts in China. Although Mo and Pb-Zn deposits are locally closely related in space in the GHR, it is disputed whether the Mo and Pb-Zn deposits have a genetic relationship. The Diyanqinamu Mo deposit located at the middle part of the northern GHR is a Late Jurassic large porphyry Mo deposit and closely adjacent by vein-type Pb-Zn deposit. In this work, we discussed the relationship between Mo and Pb-Zn deposits in Diyanqinamu mine based on the data of S and Pb isotopic geochemistry and geological information. In this mine, the Mo deposit is concentrated in the southern area with a distance of 500 m to the vein Pb-Zn deposit. The $\delta^{34}S_{CDT}$ values of the galena and sphalerite from the Mo deposit range from +1.73‰ to +7.29‰ with average of +5.04‰. By contrast, $\delta^{34}S_{CDT}$ values of the galena and sphalerite from the Pb-Zn deposit, ranging from +2.38‰ to +5.46‰ with average of +4.04‰, is similar to that of the Mo deposit. The formation temperatures of the Pb-Zn deposit calculated based on the sulfur isotope balance fractionation between sphalerite and co-existed galena range from 220 °C to 315 °C (average 247 °C), which is lower than that of the Mo mineralization (292–510 °C). Pb isotopic results show that the $^{206}Pb/^{204}Pb$, $^{207}Pb/^{204}Pb$, and $^{208}Pb/^{204}Pb$ values of the Pb-Zn deposit range from 18.326–18.364, 15.541–15.589, and 38.054–38.214, respectively, which are slightly higher than those of the Mo deposit ranging from 18.287–18.331, 15.532–15.569, and 38.034–38.139, respectively. In the $^{206}Pb/^{204}Pb$-$^{207}Pb/^{204}Pb$ diagram, sulfides sampled from the Mo and Pb-Zn deposits overlapped with each other and formed a linear distribution, indicating that they are derived from a mixed metal source with more external contribution to the Pb-Zn mineralization. This mixed signal is further confirmed by the geologic facts that the host rocks of the vein-type Pb-Zn deposit have abnormally high contents of Pb, Zn, and Ag, and experienced strong hydrothermal alteration. Combined with the ore geology, mineral assemblage, and isotopic geochemistry of the two types of mineralization, we propose that the Mo and Pb-Zn deposits in the Diyanqinamu mine represent different faces of the same porphyry system. This Mo-Pb-Zn metallogenic system would provide important clues on further prospecting of Mo and Pb-Zn resources in the GHR.

Keywords: vein-type Pb-Zn deposit; Diyanqinamu porphyry Mo deposit; Great Hinggan Range; S and Pb isotope

1. Introduction

The Great Hinggan Range (GHR) in the easternmost Central Asian Orogenic Belt (CAOB) is one of the most important polymetallic metallogenic belts in China (Figure 1), which hosts a great many of Mo,

Sn, Au, Cu, Ag, Pb, and Zn deposits [1–6]. Many studies have been carried out on the genesis of Mo deposits [7–11]. However, the genesis of vein-type Pb-Zn deposits spatially associated with Mo deposit are poorly constraint. Vein-type Pb-Zn deposits are commonly associated with Cu-Mo mineralization in porphyry deposits, such as MAX porphyry Mo deposit [12] and Donggou porphyry Mo deposit [13–15] and are considered as part of the porphyry system [16,17]. It is still disputed whether the Pb-Zn and Mo deposits in the GHR have a genetic relationship. Although some scholars suggested that these peripheral Pb-Zn deposits may represent distal faces of the porphyry system [18,19], and many researchers classified them as hydrothermal vein-type deposits, their origin is still constrained poorly in detail [1,20–22].
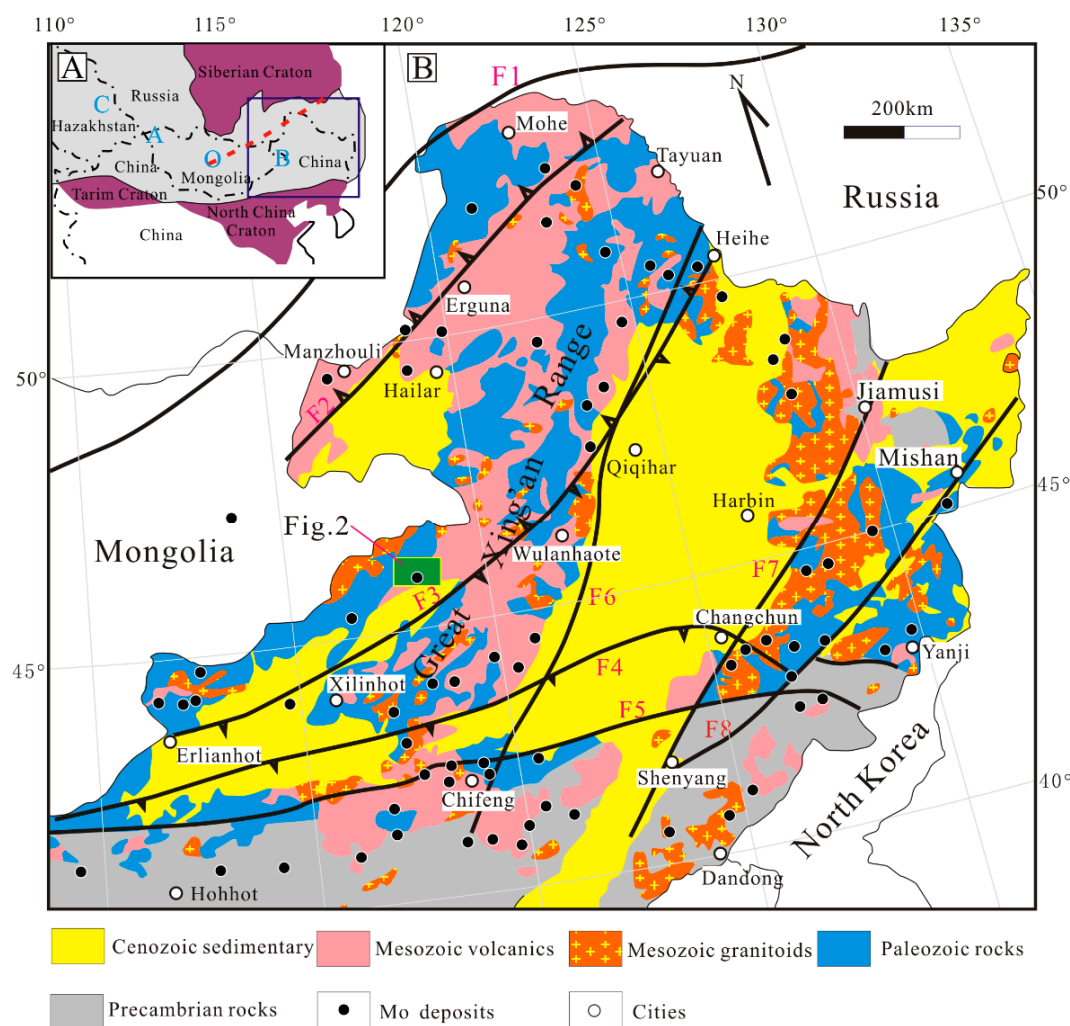

Figure 1. Distribution of the Mesozoic granitoids and Mo deposits in the Great Hinggan Range (GHR) and adjacent area. F1: Mongolia–Okhotsk suture belt; F2: Derbugan fault; F3: Erlian–Hegenshan Fault; F4: Xilamulun river fault; F5: Kangbao–Chifeng fault; F6: Nenjiang fault; F7: Yilan–Yitong fault; F8: Dunmi fault. CAOB: Central Asian Orogenic Belt. (**A**) Simplified tectonic map of CAOB showing major tectonic phases surrounding the GHR (modified after [2]). (**B**) Simplified geologic map of the GHR and its adjacent areas (modified after [9,23,24]).

Isotope geochemistry is a powerful tool to determine the sources of ore-forming fluids and melts in hydrothermal deposits. Sulfur isotope has been widely applied to constrain the genesis of hydrothermal deposits [25,26]; lead isotope is a significant monitor for tracing sources of hydrothermal fluids and their migration paths [26–28].

The Diyanqinamu Mo deposit in the middle part of northern GHR contains a proven reserve of 0.79 Mt Mo metal with an average grade of 0.099% (Figure 1B) [23]. The vein-type Pb-Zn deposit adjacent to the Mo deposit contains 50,100 t Pb + Zn ore reserves with mean grades of 2.61 wt% Pb, 3.04 wt% Zn, and Ag resource 0.94 t at 106 g/t (Figure 2) [29]. Previous studies mostly focused on the Mo deposit in alteration [30], metal sources [31], the ore genesis and tectonic setting [2,24,32], however, the genetic relationship between porphyry Mo and vein Pb-Zn deposits is poorly studied. In order to probe their genetic relationship, detailed geological and geochemical studies have been carried out on the vein-type Pb-Zn and porphyry Mo deposits in the Diyanqinamu mine.
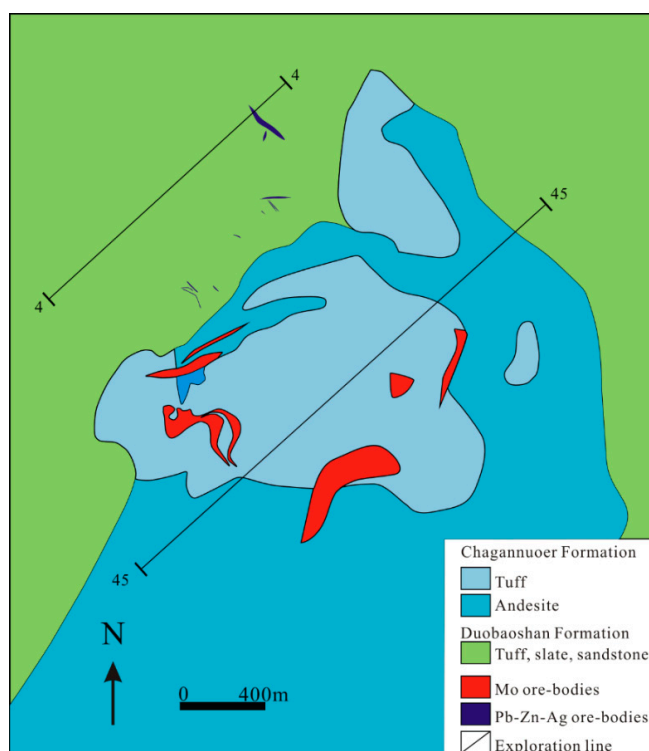

Figure 2. Geologic map of the Diyanqinamu mine (Modified after [24,32]).

In this paper, we present new S-Pb isotopic compositions of sulfide minerals from both deposits. Combined with previous results, we propose that the vein-type Pb-Zn deposit is a distal face of the porphyry Mo deposit in Diyanqinamu mine. This Mo-Pb-Zn metallogenic system would provide important clues on further prospecting of Mo and Pb-Zn resources in the GHR.

2. Regional Geology

The GHR is one part of the eastern CAOB between the Siberian Craton and the North China Craton (Figure 1) [33,34], and a NE–SW-trending tectonic domain that is bordered by the Xar–Moron Fault to the south, the Mongol–Okhotsk suture zone to the north, and the Songliao Basin to the east [6]. The GHR experienced a long and complex tectonic evolution from the Paleozoic to Mesozoic [5,6]. During the Paleozoic, the GHR experienced multiple collision and suture between Siberia and North China Cratons which is mainly controlled by tectonic evolution of the Paleo Asian Ocean [34]. During the Mesozoic, the GHR successively overprinted by a prolonged complicated tectonic of Mongolia–Okhotsk Ocean tectonic domain in the north [35–38], and circle Paleo–Pacific Ocean tectonic domain in the east [39,40] and/or lithosphere thinning process [41]. Accordingly, this area exposed widespread Mesozoic igneous rocks with positive εNd(t) and young Nd model ages, which mostly formed during the Late Jurassic to the Early Cretaceous and constitutes one of the largest plutonic provinces in the world [34,39,42,43]. Many of these plutons are fertile and constitute the GHR

metallogenic province [44]. Four pulses of Mo metallogenic events of 250–200 Ma, 200–160 Ma, 160–130 Ma, and <130 Ma (130–100 Ma) have been identified in the GHR [9].

The middle part of northern GHR within Chinese territory is bordered by the Erlian–Hegenshan fault in the south (Figure 1B). Paleozoic and Mesozoic rocks are discontinuously exposed and the Precambrian rocks are largely absent [45]. The Paleozoic strata are composed mainly of the Ordovician intermediate-acid volcanics interbedded with clastic rocks, the Devonian and Carboniferous clastic rocks, and Permian intermediate-acid volcanics with interlayers of bioclastic limestone [23,46]. The Mesozoic strata overlying uncomfortably on the Paleozoic strata are composed mainly of Jurassic volcaniclastic rocks intercalated with mafic volcanic and sedimentary rocks, and Cretaceous sandstone, mudstone, and conglomerate with interlayers of lignite, without the Triassic rocks [23,46]. Many of the Paleozoic and Mesozoic granites are fertile and are considered to be closely related to various mineral resources [7,9,47–49].

3. Ore Deposit Geology

The strata in the Diyanqinamu mine consist mainly of Duobaoshan Formation and Chagannuoer Formation (Figure 2). The Duobaoshan Formation emplaced at Middle Ordovician and consists of weak metamorphic rocks, such as tuffaceous slab and tuffaceous sandstone. The Chagannuoer Formation is composed of tuff, andesite, basalt, dacite, and pyroclastic rock [23,24]. Recently, LA-ICPMS zircon U-Pb chronological results indicated that the basalt of Chagannuoer Formation emplaced at 260 ± 4.0 Ma [50]. This age is earlier than Late Jurassic as previously considered [30,31,51]. The Diyanqinamu area was subjected to intensive tectonic and magmatic activities [49]. NE- (F2, F3 and F4) and NW-trending faults (F1, F2) controlled the morphology of the Mo ore-bodies. The intrusive bodies are porphyritic granites, discovered in the drill holes ZK9701 and ZK8502, and aplitic granites penetrated in drill holes ZK4522 and ZKp2104 [32]. These granites are located in the southeast quadrant of the Diyanqinamu mine, intruded the andesite, basalt, and volcaniclastic (Figure 3). Both porphyritic granites and aplitic granites are high-K calc-alkaline and highly fractionated I-type granites [32]. Petrography shows that the granites experienced fluid exsolution, as demonstrated by the corroded quartz in the porphyritic granites, skeletal quartz in the aplitic granites, and the unidirectional solidification texture (UST) in the apex of the aplitic granites [23].
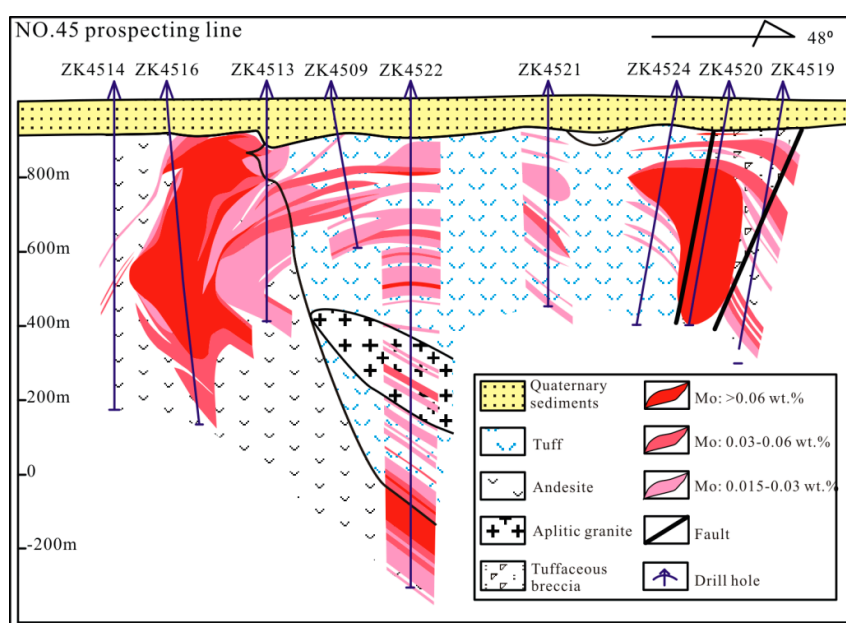

Figure 3. Geological profile of exploration line 45 in the Diyanqinamu mine.

In the Diyanqinamu mine, vein-type Pb-Zn deposit occurs in close proximity of the porphyry Mo deposit, displaying a Mo-Pb-Zn mineralization distribution pattern (Figure 2). The Pb-Zn deposit is about 500 m to the porphyry Mo deposit in this mine (Figure 2).

3.1. Mo Sulfide Deposit

The Mo deposit mainly consists of three Mo ore-bodies, and most of them are concentrated in the andesite and volcaniclastic rocks. Overall, ore-bodies are barrel- and diamond-shaped at depth and plan, respectively, with most of them located at above 400 m elevation, whereas individual ore-body in some places may reach −250 m elevation at depth such as drill holes ZK4111 and ZK4522 (Figure 3) [23].

Molybdenum mineralization is dominated by veins, disseminated grains, banded and fracture infills (Figure 4a–f) [24]. The main ore minerals are molybdenite and pyrite, with minor chalcopyrite, galena, sphalerite, bismuthinite, and arsenopyrite. In addition, magnetite presenting in the early barren and fertile stage indicate that the hydrothermal fluids are relatively oxidized at the early stage (Figure 4f) [23]. As subordinate sulfide phase, sphalerite presents during and after Mo mineralization. According to their mineral association, three generations of sphalerite could be primarily discerned (Figure 4g−i). Sphalerite-i is fine grained coexisting with molybdenite (Figure 4g); Sphalerite-ii presents as fine grains enclosed in pyrite (Figure 4h); Sphalerite-iii shows granular texture coexisting with galena, pyrite, quartz, and carbonates minerals (Figure 4i). Compared to sphalerite, galena is minor with fine granular texture and coexisting with sphalerite and pyrite (Figure 5i). The main gangue minerals are quartz, feldspar, sericite, fluorite, and calcite. The results of LA-ICPMS zircon U-Pb and molybdenite Re-Os of this Mo deposit yield metallogenic age of ca. 156 Ma [24,32].
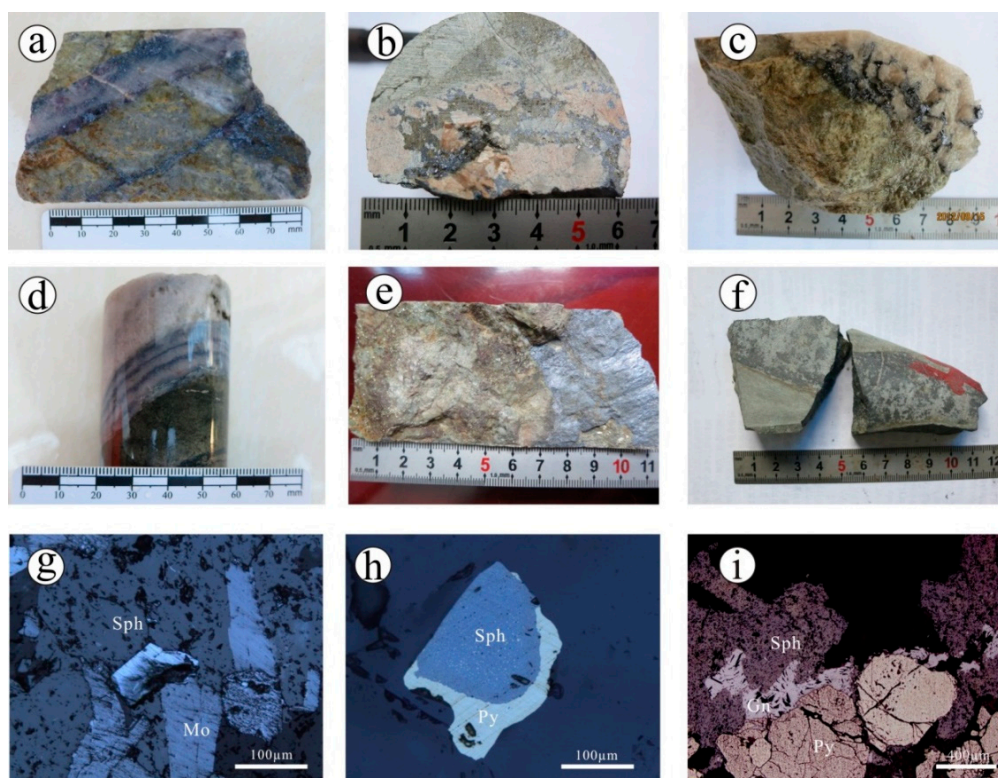

Figure 4. Photographs and photomicrographs showing ore geology of the Mo deposit in Diyanqinamu mine. (**a**): Veined molybdenite-fluorite-quartz ore; (**b**): veined molybdenite-K-feldspar-quartz ore; (**c**): veined molybdenite-quartz ore; (**d**): banded molybdenite-quartz ore; (**e**): molybdenite film in fracture; (**f**): veined molybdenite-quartz-magnetite ore; (**g**): sphalerite coexists with molybdenite; (**h**): sphalerite with chalcopyrite disease structure metasomatismed by pyrite; (**i**): sphalerite coexists with pyrite and galena. Gn: Gelana; Sph: Sphalerite; Mo: Molybdenite; Py: Pyrite.
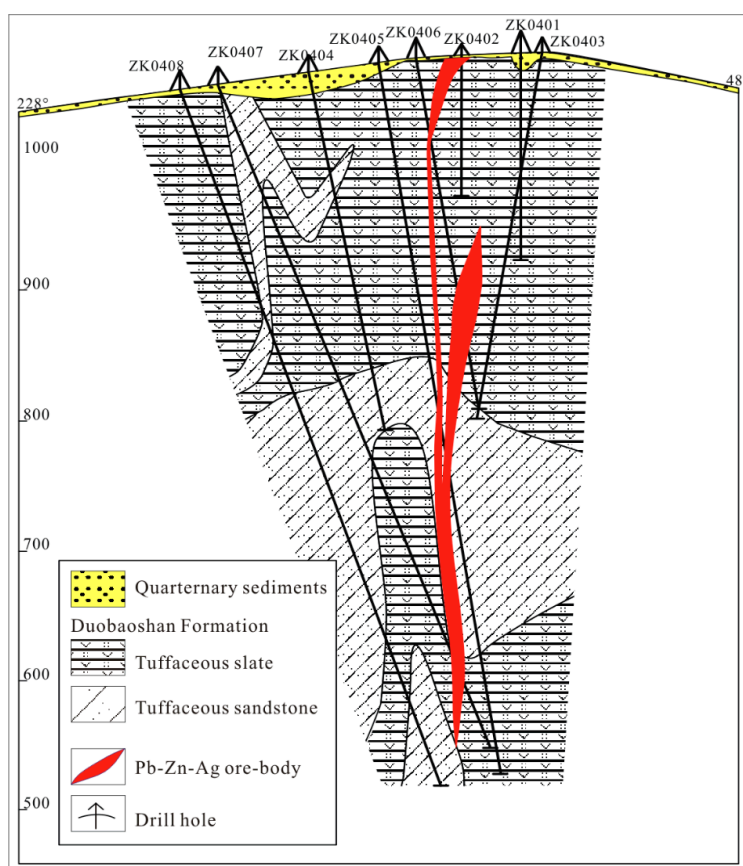
Figure 5. Geological profile of exploration line 04 for Pb-Zn vein ores in the Diyanqinamu mine (modified from [29]).

Hydrothermal alteration is well developed in both the concealed porphyry and the volcanic rocks. The dominated alteration types are potassic alteration, silification, phyllic, and propylitic alteration [23,24,52]. Based on field and microscopic observations on the crosscutting relationships of various veins and paragenetic relationships of hydrothermal minerals, four stages of hydrothermal veins have been identified. Stage I is composed of quartz and K-feldspar, and minor molybdenite, magnetite, pyrite, epidote, and chlorite; Stage II contains predominantly quartz, fluorite, and molybdenite, and minor pyrite; Stage III is mainly composed of quartz, fluorite, pyrite, chalcopyrite, galena, sphalerite, and molybdenite; Stage IV is composed of quartz, fluorite, calcite, dolomite, galena and sphalerite, and absence of molybdenite [23,24,52]. Similar to some Mo deposits in China [11,14], fluorite alteration with diverse colors including purple, green, and white is found to be one of the most important alterations. Interestingly, the fluorites intergrowth with molybdenite are mostly purple. Combined evidence of widespread fluorite alteration, similar Sr and Nd isotopic compositions between the purple fluorite and the concealed granites, and high fluorine content of the apatite from the concealed granites, Sun et al. [23] proposed that the metallogenic granite is F-enriched, and the Mo ore-forming fluids may have been derived from this granitic magma.

3.2. Pb-Zn Sulfide Deposit

The morphology of Pb-Zn deposit adjacent to the Mo deposit in the northwest of Diyanqinamu mine is exposed by a small amount of borehole data with the extension in depth poorly constraint currently. The Pb-Zn ore-bodies occur chiefly as lenses and veins, and are concentrated mainly in the NW-trending fractures with a dip angle of 60°–70° in the weak metamorphic rocks of Duobaoshan Formation (Figure 5). The Pb-Zn deposit mainly contains of five ore-bodies containing 50,100 t Pb +

Zn ore reserves with mean grades of 2.61 wt% Pb, 3.04 wt% Zn; No. I-1 ore-body is one of the largest ore-bodies, displaying 50–100 m in length and 0.8–19 m in width [29].

The ore minerals include sphalerite, galena, pyrite, argentiferous tetrahedrite, and argentite. Sphalerite and galena display granular textures and coexist with pyrite (Figure 6a–f). It is worth noting that chalcopyrite disease structure in sphalerite is common in both the Mo and Pb-Zn ores (Figure 4g, Figure 6d–f), which may be related to the exsolution of chalcopyrite from sphalerite during cooling or replacement of original Fe-bearing sphalerite by an aggregate of chalcopyrite [53]. Gangue minerals include quartz and minor pyrolusite. Alteration assemblage are mainly kaolinization, sericitization, silification at depth, and ferritization at the surface.
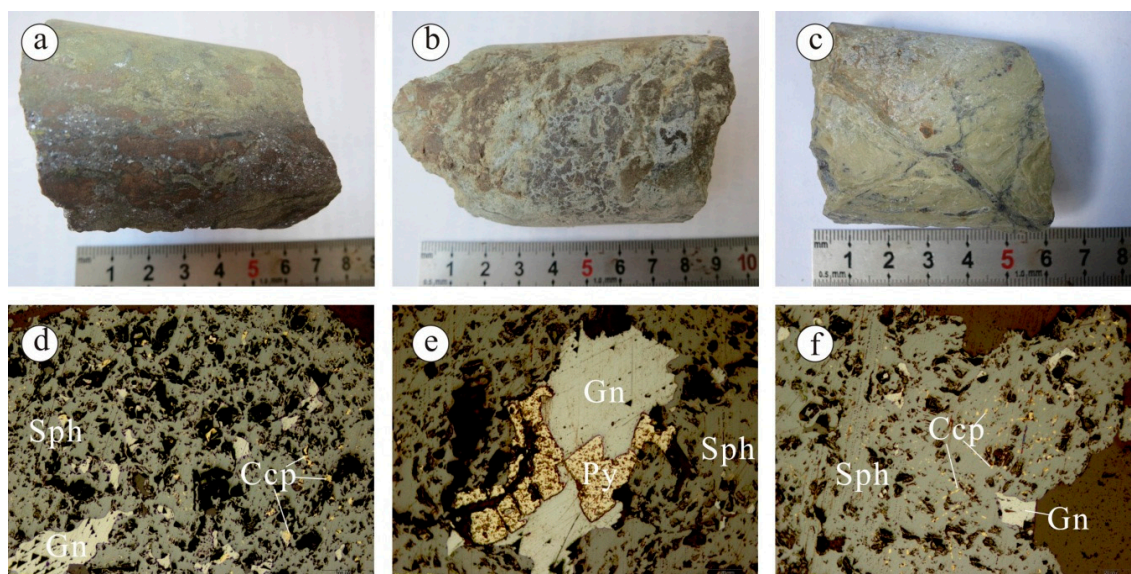

Figure 6. Photographs and photomicrographs showing ore geology of the Pb-Zn deposit in Diyanqinamu mine. (**a**): massive Pb-Zn ores; (**b**): disseminated Pb-Zn ores; (**c**): veined Pb-Zn ore; (**d**): sphalerite displaying chalcopyrite disease structure coexists with galena; (**e**): sphalerite showing chalcopyrite disease structure coexists with pyrite and galena; (**f**): sphalerite showing chalcopyrite disease structure coexists with galena. Gn: Gelana; Sph: Sphalerite; Py: Pyrite; Ccp: Chalcopyrite.

4. Analytical Methods and Samples

All the samples in this study were collected from different drill holes in the Diyanqinamu mine. Twenty-six samples were chosen for S isotopic analyses, fourteen of them from the Pb-Zn deposit and twelve from the Mo deposit. Besides, ten samples from the Pb-Zn deposit and four samples from the Mo deposit in this mine were chosen for Pb isotopic analyses. All of these minerals were separated by hand picking under a binocular microscope. Separated grains were rinsed with distilled water. After drying at 25–30 °C, the concentrations were grounded to powder for S-Pb isotope analyses.

Sulfur isotope analyses of these sulfide minerals were carried out at the State Key Laboratory of Environmental Geochemistry, Institute of Geochemistry, Chinese Academy of Sciences, by using Continuous Flow Mass Spectrometer. GBW 04415 and GBW 04414 Ag_2S were used as the external standards, and the relative errors (2σ) were better than 0.1‰ from the replication of standard materials. Sulfur isotopic compositions are reported relative to Canyon Diablo Troilite (CDT).

Lead isotope compositions were determined using ~100 mg sulfide powder that was dissolved in concentrated HF + HNO_3 for 48 h. Lead was separated and purified using diluted HBr before isotopic compositions were determined using MAT 261 mass spectrometer at the Geological Analysis Laboratory under the Ministry of Nuclear Industry, China. The precision of the $^{208}Pb/^{206}Pb$ measurements (1 μg of Pb) is ents (1 μgositions were determined using MAT 261 mass spectrometer at the Geologic$^{208}Pb/^{206}Pb$

= 36.611 ± 0.004, ^{207}Pb/^{206}Pb = 15.457 ± 0.002, and ^{204}Pb/^{206}Pb = 16.937 ± 0.002, in agreement with the reference value [54].

5. Results

The δ^{34}S$_{CDT}$ values of galena and sphalerite are listed in Table 1. In the Mo deposit, galena and sphalerite samples display wide range of δ^{34}S$_{CDT}$ values ranging from +1.73‰ to +7.29‰ (average of +5.04‰) (Figure 7). The δ^{34}S$_{CDT}$ values of galena samples range from +1.08‰ to +1.73‰ (average of +1.39‰). Sphalerite samples, by contrast, are slightly enriched in heavy sulfur isotope ranging from +4.13‰ to +7.29‰ (average of +5.46‰). In the Pb-Zn deposit, the δ^{34}S$_{CDT}$ values of galena and sphalerite samples show narrow range +2.38‰ to +5.46‰ (average of +4.04‰) (Figure 7), with the galena samples ranging from +2.38‰ to +5.21‰ (average of +3.43‰) and sphalerite samples relatively enriched in heavy sulfur isotope ranging from +4.46‰ to +5.46‰ (average of +4.94‰).

The Pb isotopic results of the sulfide samples from both of Pb-Zn and Mo deposit are listed in the Table 2. The sulfides from the Pb-Zn deposit have ^{206}Pb/^{204}Pb, ^{207}Pb/^{204}Pb, and ^{208}Pb/^{204}Pb values of 18.326–18.364, 15.541–15.589, and 38.054–38.214, respectively. Overlapping with the samples from Pb-Zn deposit in ^{206}Pb/^{204}Pb-^{207}Pb/^{204}Pb diagram (Figure 8), the sulfides from the Mo deposit, by contrast, have relatively lower Pb isotopic values, presenting ^{206}Pb/^{204}Pb, ^{207}Pb/^{204}Pb, and ^{208}Pb/^{204}Pb values of 18.287–18.331, 15.532–15.569, and 38.034–38.139, respectively.

Table 1. Sulfur isotopic composition of the sulfides from Pb-Zn and Mo deposits in the Diyanqinamu mine.

Sample no.	δ^{34}S$_{V-CDT}$‰		T/°C	Sample Location
	Sphalerite	Galena		
ZK0643-6	4.83 ± 0.03	2.92 ± 0.01	230	
ZK0643-7	4.79 ± 0.08	3.11 ± 0.03	245	
ZK0643-8	4.47 ± 0.04	2.38 ± 0.01	220	
ZK0643-9	4.87 ± 0.04	2.96 ± 0.08	230	Pb-Zn deposit
ZK0643-13	4.46 ± 0.13	3.45 ± 0.01	315	
ZK0643-15	5.41 ± 0.02	3.74 ± 0.02	246	
ZK0643-16	5.46 ± 0.02	3.70 ± 0.02	239	
ZK5304-33	3.25 ± 0.19	1.73 ± 0.02	258	
ZK3734-6		1.39 ± 0.01		
ZK3734-20		1.35 ± 0.01		
ZK5304-34		1.08 ± 0.05		
ZK5304-14	5.94 ± 0.01			
ZK3734-2	7.29 ± 0.05			Mo deposit
ZK3734-19	5.04 ± 0.02			
ZK6115-10	4.13 ± 0.07			
ZK3314-12	6.53 ± 0.02			
ZK3314-9	6.63 ± 0.03			
ZK4107-3	4.86 ± 0.05			

Sp: sphalerite; Gn: galena. The balance fractionation equation of sphalerite-galena mineral pair based on Ohmoto et al. [55]: $1000\ln\alpha = (1.01 \pm 0.04) \times 10^5/T^2$.
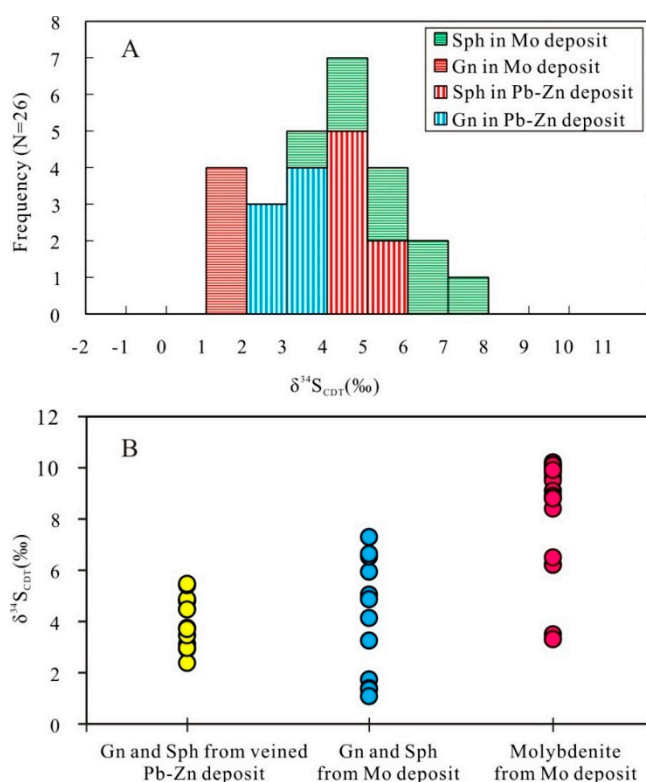
Figure 7. Sulfur isotope histogram of galena and sphalerite sampled from Mo and adjacent vein-type Pb-Zn deposits in the Diyanqinamu mine. Sulfur isotopic data of the molybdenite separates from Mo ores are quoted from [24]. Mineral abbreviations are the same as those in Figure 6. (**A**) S isotopic histogram of sulfides from the Mo and Pb-Zn deposits in the Diyanqinamu mine. (**B**) δ^{34}S values of various sulfides from the Mo and Pb-Zn deposits in the Diyanqinamu mine.

Table 2. Lead isotopic composition of sulfides from Mo and Pb-Zn deposits in the Diyanqinamu mine.

Sample no.	Mineral	^{208}Pb/^{204}Pb	Std Err	^{207}Pb/^{204}Pb	Std Err	^{206}Pb/^{204}Pb	Std Err	Ore Type
ZK0643-6		38.054	0.003	15.541	0.001	18.326	0.001	
ZK0643-14		38.114	0.004	15.558	0.003	18.339	0.003	
ZK0643-13	Gn	38.112	0.002	15.560	0.001	18.336	0.001	
ZK0643-15		38.102	0.003	15.556	0.001	18.333	0.001	
ZK0643-16		38.201	0.004	15.587	0.002	18.359	0.002	Pb-Zn ores
ZK0643-6		38.168	0.006	15.577	0.002	18.353	0.003	
ZK0643-13		38.138	0.003	15.565	0.001	18.347	0.002	
ZK0643-14	Sph	38.214	0.005	15.589	0.002	18.364	0.002	
ZK0643-15		38.123	0.004	15.562	0.002	18.339	0.002	
ZK0643-16		38.169	0.004	15.576	0.003	18.356	0.003	
ZK3734-6	Gn	38.072	0.005	15.554	0.002	18.287	0.002	
ZK5304-34		38.080	0.003	15.548	0.001	18.323	0.001	Mo ores
ZK3734-19	Sph	38.034	0.004	15.532	0.002	18.319	0.002	
ZK5304-33		38.139	0.004	15.569	0.002	18.331	0.002	

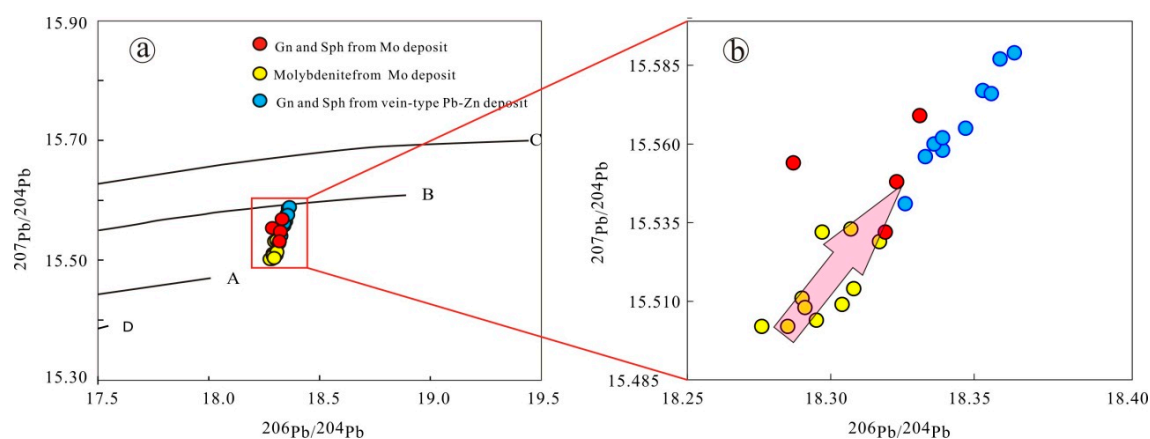Mineral abbreviations are same to those in Table 1.

Figure 8. Sulfide Pb composition of both porphyry Mo and adjacent vein-type Pb-Zn deposits in the Diyanqinamu mine. Trends for the Upper Crust (C), Orogenic Belt (B), Mantle (A) and Lower Crust (D) are from Zartman and Doe [56]. Lead isotopic data of the molybdenite separates in Mo ores from Leng et al. [24]. Mineral abbreviations are the same as those in Figure 5. (**a**) Two-stage Pb isotope evolution diagram for sulfides from the Mo and Pb-Zn deposits in the Diyanqinamu mine. (**b**) $^{206}Pb/^{204}Pb$ versus $^{207}Pb/^{204}Pb$ diagram.

6. Discussion

6.1. Possible Source of Sulfur

The vein-type Pb-Zn deposit is located about 500 m northwest of the porphyry Mo deposit in Diyanqinamu mine (Figure 2). Both deposits in this mine have simple sulfide mineral assembly, mainly composed of molybdenite, pyrite, galena, and sphalerite with molybdenite absent in the Pb-Zn deposit. The lack of sulfate minerals suggests that the sulfide $\delta^{34}S$ values can trace the $\delta^{34}S$ values of the ore-forming fluids [55,57,58]. All galena and sphalerite samples from Pb-Zn deposit have homogenous $\delta^{34}S_{CDT}$ values ranging from +2.38‰ to +5.21‰ and +4.46‰ to +5.46‰, respectively (Table 1 and Figure 7). Galena and sphalerite samples from the Mo deposit have a wide range of $\delta^{34}S_{CDT}$ values, ranging from +1.08‰ to +1.73‰ and +4.13‰ to +7.29‰, respectively (Table 1 and Figure 7). Overall, the $\delta^{34}S$ values of galena and sphalerite samples from both deposits are broadly similar to those of molybdenite from the Diyanqinamu mine (ranging from +3.3‰ to +10.2‰ with average of +8.2‰ [24]) (Figure 7B). Because no marine evaporites or carbonates are in this region, these relatively high $\delta^{34}S$ values of the sulfides from the Mo deposit in the Diyanqinamu mine have been suggested could be inherited from a magmatic source [24], which is also supported by the evidence that the fluorite coexisting with molybdenite presents similar Sr and Nd isotopic composition to the concealed high-F granite [23]. Therefore, in the Diyanqinamu mine, the $\delta^{34}S$ values of the sulfide samples from the Pb-Zn deposit present overlap with those of the Mo deposit (Figure 7), suggesting that the two deposits have a common S source.

In addition, all $\delta^{34}S$ values of galena and sphalerite samples from Pb-Zn deposit are characterized by $\delta^{34}S_{sphalerite} > \delta^{34}S_{galena}$. Under microscope, these galena and sphalerite coexisted with each other (Figure 5). These lines of evidence suggest that the S isotope fractionation has reached equilibrium in hydrothermal fluids. The formation temperatures calculated based on the sulfur isotope balance fractionation between sphalerite and coexisted galena range from 220 °C to 315 °C with average temperature of 247°C (Table 1) which is lower than the formation temperature of Mo mineralization (292–510°C, [52]). Therefore, the S isotopic data and other evidence imply that the Mo and Pb-Zn deposits in the Diyanqinamu mine share a common S source and present the descending temperature of the hydrothermal fluid.

6.2. Origin of Ore-forming Metals

Sulfides generally have very low U and Th contents, and hence their radiogenic Pb are negligible and age correction is not needed. Therefore, the lead isotopic compositions of sulfide samples in the Diyanqinamu could inherit source signals of ore-forming metals. The lead isotopic data of galena, sphalerite, and molybdenite from Mo and Pb-Zn deposits in the Diyanqinamu are distributed between the orogenic belt and mantle average evolution curves in the ^{207}Pb/^{204}Pb vs. ^{206}Pb/^{204}Pb diagram, and form an elongate narrow trend (Figure 8, [56]). These sulfide samples from the Mo deposit are characterized by overlapping with each other in ^{206}Pb/^{204}Pb and ^{207}Pb/^{204}Pb ratios, with the molybdenite showing much lower values than those of galena and sphalerite (Figure 8B). Previous works on the Pb isotope proved that the ore-forming metals of Mo mineralization were predominantly derived from granitic magma [23,24]. In contrast, the sphalerite and galena samples from the Pb-Zn deposit in this mine display much higher ^{206}Pb/^{204}Pb and ^{207}Pb/^{204}Pb ratios, and well overlap with those of the sphalerite and galena samples from the Mo deposit. The variation in Pb isotope may be resulted from a mixing of two or more isotopically distinct sources in the ore-forming process. This prediction is broadly confirmed by the fluid inclusion analyses and H-O isotope variation, which indicates that fluid mixing existed during the late stage of the Mo mineralization [52]. In addition, S isotopic data above suggest that the galena and sphalerite from the Mo and the Pb-Zn deposits in the Diyanqinamu mine are most likely of magmatic hydrothermal origin [23,24]. Therefore, mixing of a magmatic fluid possessing low ^{206}Pb/^{204}Pb and ^{207}Pb/^{204}Pb ratios with isotopically evolved crustal materials of high corresponding ratios would be a plausible explanation. The sulfides from the Pb-Zn deposit exhibiting higher ^{208}Pb/^{204}Pb and ^{207}Pb/^{204}Pb ratios represent a mixed source with more external material. This speculation is also consistent with the geology fact that the fresh rocks of Duobaoshan Formation, as the host rocks of Pb-Zn ore-bodies, are characterized by high abundance of Pb, Zn, and Ag [59]. The strong kaolinization, sericitization, and silification alteration of these rocks could promote the leaching of Pb, Zn, and Ag from the host rocks, leading to the enhancement of the metallogenic potential for Pb-Zn deposit subsequently.

6.3. Genesis of Diyanqinamu Mo-Pb-Zn Polymetallic Deposit

Many porphyry districts in the world exhibit close association in space between the porphyry Mo deposit and vein-type Pb-Zn deposit [12,17]. At Climax Mo deposit in USA, East Qinling molybdenum belt in China, and MAX Mo deposit in Canada, vein-type Pb-Zn deposits have been suggested to be a distal member of the porphyry system [12,14,15]. A continuum hydrothermal evolution model was proposed by Silitoe [60] to explain this close spatial relationship between vein-type Pb-Zn and porphyry Mo deposits. Lawley et al. [12] suggested that porphyry deposit is genetically related to a wide range of deposit types, including skarn, base, and precious metal veins, and epithermal precious-metal deposits.

In the Diyanqinamu mine, the vein-type Pb-Zn deposit are close to the porphyry Mo deposit in space with a short distance of about 500 m. In mineral assemblage, many galena and sphalerite were present during and after the Mo mineralization. S and Pb isotope data of galena and sphalerite in both the Pb-Zn and Mo deposits show that they share similar S and metal sources. Although the formation temperature of Pb-Zn mineralization is lower than the fluid inclusion homogenization temperature of molybdenite-bearing quartz vein [52], this evolution trend of temperature is consistent with metal zonation typically observed in a porphyry-related hydrothermal system [17]. Therefore, it is reasonable to infer that the temperature discrepancy between Mo and Pb-Zn mineralization reflects the evolution of the hydrothermal fluids. That is, during the late evolution stage of granitic magma, there existed exsolution of a high-temperature, F-rich, and high-fO$_2$ ore-bearing hydrothermal fluids. According to the results of microscopic temperature measurement of inclusions and H-O isotope, this hydrothermal fluid experienced at least three stages of fluid boiling during the evolution of hydrothermal veins from Stage I to Stage III and was diluted by meteoric water, leading to the deposition of molybdenite as veins or infills along the fractures adjacent to the concealed granite [23,52]. As the migration of this

hydrothermal fluid, the fluid could extract some metals from the host rocks, such as the Duobaoshan Formation, through convective circulation, meanwhile, lead to the strong hydrothermal alterations and the enhanced capability of the Pb-Zn mineralization subsequently. Thus, the Mo and Pb-Zn deposits in the Diyanqinamu mine represent different faces of the same porphyry system. As more and more Mo and Pb-Zn deposits are discovered in the north of GHR (e.g. [1,61]), in this case, the view of Mo-Pb-Zn metallogenic system has significant implication for Mo and Pb-Zn mineral exploration in this area.

7. Conclusions

In the Diyanqinamu mine, the vein-type Pb-Zn deposit is closely adjacent to the porphyry Mo deposit in space. Sulfides from both Mo and Pb-Zn deposits in this mine have similar $\delta^{34}S$ values and show magmatic origin. The formation temperature of the coexisted galena and sphalerite based on S isotopic data of galena-sphalerite pairs for Pb-Zn deposits is lower than the fluid inclusion homogenization temperature of the molybdenite-bearing quartz vein. Lead isotopic data from both of Mo and Pb-Zn deposits are characterized by an evolution trend, with the molybdenite showing lower values, and the galena and sphalerite showing higher ratios. This kind of Pb isotopic signature suggests that both deposits share a mixed metal source, with more material from the host rocks for the Pb-Zn deposits. Combined with the previous research results and our work this time, we suggest that the Mo and Pb-Zn deposits in the Diyanqinamu mine consist of a zoned magmatic hydrothermal system. The association of Mo and Pb-Zn deposits, in this case, could provide an important exploration indicator for each other, and would discharge important information for the regional mineral exploration.

References

1. Zhang, K.; Jin, R.S.; Sun, F.Y.; Li, B.; He, P.; Zhang, Y.L.; Guo, S.; Zhang, T.F. Metallogenesis and ore-forming time of the Changtuxili Mn–Ag–Pb–Zn deposit in Inner Mongolia: Evidence from C–O–S isotopes and U–Pb geochronology. *Geosci. Front.* **2019**, *11*, 13. [CrossRef]

2. Sun, H.R.; Yan, G.S.; Lv, Z.C.; Yu, X.F.; Li, Y.S.; Gong, F.Y. Analysis of the spatial and temporal distribution and metallogical background of molybdenum deposits in Northeast China. *China Min. Mag.* **2016**, *S1*, 189–196. (in Chinese with English abstract)

3. Liu, J.M.; Zhang, R.; Zhang, Q.Z. The regional metallogeny of Da Hinggan ling, China. *Earth Sci. Front.* **2004**, *11*, 269–277. (in Chinese with English abstract)

4. Wang, J.B.; Wang, Y.W.; Wang, L.J. Copper metalogenic setting and prospecting potential in the middle southern part of Da Hinggan Moutains. *Geol. Prospect.* **2000**, *36*, 1–4. (in Chinese with English abstract)

5. Zeng, Q.D.; Liu, J.M.; Chu, S.X.; Guo, Y.P.; Guo, S.; Guo, L.X.; Zhai, Y.Y. Poly-Metal Mineralization and Exploration Potential in Southern Segment of the Da Hinggan Mountains. *J. Jilin Univ. Earth Sci. Ed.* **2016**, *46*, 1100–1123. (in Chinese with English abstract)

6. Bai, L.A.; Sun, J.G.; Gu, A.L.; Zhao, K.Q.; Sun, Q.L. A review of the genesis, geochronology, and geological significance of hydrothermal copper and associated metals deposits in the Great Xing'an Range, NE China. *Ore Geol. Rev.* **2014**, *61*, 192–203. [CrossRef]

7. Ouyang, H.; Mao, J.W.; Hu, R.Z. Geochemistry and Crystallization Conditions of Magmas Related to Porphyry Mo Mineralization in Northeastern China. *Econ. Geol.* **2020**, *115*, 79–100. [CrossRef]

8. Zhou, Z.H.; Gao, X.; Ouyang, H.G.; Liu, J.; Zhao, J.Q. Formation mechanism and intrinsic genetic relationship between tin-tungstenlithium mineralization and peripheral lead-zinc-silver-copper mineralization:

Exemplified by Weilasituo tin-tungsten-lithium polymetallic deposit, Inner Mongolia. *Miner. Depos.* **2019**, *38*, 1004–1022.

9. Chen, Y.J.; Zhang, C.; Wang, P.; Pirajno, F.; Li, N. The Mo deposits of Northeast China: A powerful indicator of tectonic settings and associated evolutionary trends. *Ore Geol. Rev.* **2017**, *81*, 602–640. [CrossRef]

10. Wang, C.N.; Wang, Q.M.; Yu, X.F.; Han, Z.Z. Metallognetic Characteristics of Tin and Ore-Search Prospect in the Southern Part of Da Hinggan Mountains. *Geol. Explor.* **2016**, *52*, 220–227. (in Chinese with English abstract)

11. Chen, Y.J.; Pirajno, F.; Li, N.; Deng, X.H. Molybdenum deposits in China. *Ore Geol. Rev.* **2017**, *81*, 401–404. [CrossRef]

12. Lawley, C.J.M.; Richards, J.P.; Anderson, R.G.; Creaser, R.A.; Heaman, L.M. Geochronology and Geochemistry of the MAX Porphyry Mo Deposit and its Relationship to Pb-Zn-Ag Mineralization, Kootenay Arc, Southeastern British Columbia, Canada. *Econ. Geol.* **2010**, *105*, 1113–1142. [CrossRef]

13. Mao, J.W.; Zhang, J.D.; Pirajno, F.; Ishiyama, D.; Su, H.M.; Guo, C.L.; Chen, Y.C. Porphyry Cu–Au–Mo–epithermal Ag–Pb–Zn–distal hydrothermal Au deposits in the Dexing area, Jiangxi province, East China—A linked ore system. *Ore Geol. Rev.* **2011**, *43*, 203–216. [CrossRef]

14. Jin, C.; Chen, W.T.; Gao, X.Y.; Li, X.C.; Bao, Z.W.; Zhao, T.P. Origin of the Wangpingxigou Pb-Zn deposit in East Qinling orogenic belt, China: Distal response to the giant Donggou porphyry Mo system? *Ore Geol. Rev.* **2019**, *109*, 101–116. [CrossRef]

15. Li, Z.K.; Bi, S.J.; Li, J.W.; Zhang, W.; Cooke, D.R.; Selby, D. Distal Pb-Zn-Ag veins associated with the world-class Donggou porphyry Mo deposit, southern North China craton. *Ore Geol. Rev.* **2017**, *82*, 232–251. [CrossRef]

16. Mao, J.W.; Ye, H.S.; Wang, T.Y.; Dai, J.Z.; Jian, W.; Xiang, J.F.; Zhou, K.; Meng, F. Mineral deposit model of Mesozoic porphyry Mo and vein-type Pb-Zn-Ag ore deposits in the eastern Qinling, Central China and its implication for prospecting. *Geol. Bull. China* **2009**, *28*, 72–79. (in Chinese with English abstract)

17. Sillitoe, R.H. Porphyry Copper Systems. *Econ. Geol.* **2010**, *105*, 3–41. [CrossRef]

18. Xie, Y.L.; Wang, C.; Ji, Y.G.; Li, L.M.; Li, Y.X.; Tang, Y.W. Porphyry Mo (W)-Epithermal Pb-Zn (Ag) metallogenic system inDongwuqi area, Inner Mongolia. *Acta Mineral. Sin.* **2015**, *S1*, 81. (in Chinese)

19. Yang, M.Z.; Hou, K.; Lu, J.P.; Jiang, F.; Fu, J.J. Chronology of Molybdenum-Lead-Zinc Polymetallic Deposit of Suo Naga, Dong Ujimqin Banner Region. *Earth Sci. J. China Univ. Geosci.* 2012; 37, 1327–1337. (in Chinese with English abstract)

20. Yu, Y.A.; Liu, H.L.; Li, J.M.; Ma, X.; Chao, Y.Y.; Li, Y.W.; Yang, W.G. Discovery and Enlightenment of the Large-Scale Polymetallic Mineralization Belt in Ajile, Inner Mongolia. *Gelogly Prospect.* **2010**, *46*, 798–804. (in Chinese with English abstract)

21. Tian, J.X. Ore-controlling structure in Dasaituo Pb-Zn camp, Dong Ujimqin Banner. *Contrib. Geol. Miner. Resour. Res.* **2005**, *20*, 102–105. (in Chinese with English abstract)

22. Jia, L.Q.; Wang, Z.H.; Xu, W.Y.; Wang, L.; Li, H.; Chang, C.J. Geological and Geochemical Characteristics and Genesis of Silver-Lead-Zinc Deposit at 1017 Highland in Dong Ujimqin Banner, Inner Mongolia. *Geol. Explor.* **2014**, *50*, 550–563. (in Chinese with English abstract)

23. Sun, H.R.; Huang, Z.L.; Li, W.B.; Ye, L.; Zhou, J.X. Geochronological, isotopic and mineral geochemical constraints on the genesis of the Diyanqinamu Mo deposit, Inner Mongolia, China. *Ore Geol. Rev.* **2015**, *65*, 70–83. [CrossRef]

24. Leng, C.B.; Zhang, X.C.; Huang, Z.L.; Huang, Q.Y.; Wang, S.X.; Ma, D.Y.; Luo, T.Y.; Li, C.; Li, W.B. Geology, Re-Os ages, sulfur and lead isotopes of the Diyanqinamu porphyry Mo deposit, Inner Mongolia, NE China. *Econ. Geol.* **2015**, *110*, 557–574. [CrossRef]

25. Ohmoto, H.; Goldhaber, M.B. Sulfur and Carbon Isotopes. In *Geochemistry of Hydrothermal Ore Deposits*, 3rd ed.; Barnes, H.L., Ed.; Wiley: New York, NY, USA, 1997.

26. Zhou, J.X.; Huang, Z.L.; Zhou, M.F.; Li, X.B.; Jin, Z.G. Constraints of C–O–S–Pb isotope compositions and Rb–Sr isotopic age on the origin of the Tianqiao carbonate-hosted Pb–Zn deposit, SW China. *Ore Geol. Rev.* **2013**, *53*, 77–92. [CrossRef]

27. Carr, G.R.; Dean, J.A.; Suppel, D.W.; Heithersay, P.S. Precise lead isotope fingerprinting of hydrothermal activity associated with Ordovician to carboniferous metallogenic events in the Lachlan fold belt of New South Wales. *Econ. Geol. Bull. Soc.* **1995**, *90*, 1467–1505. [CrossRef]

28. Zhou, C.X.; Wei, C.S.; Guo, J.Y.; Li, C.Y. The source of metals in the Qilinchang Zn-Pb deposit, northeastern Yunnan, China: Pb-Sr isotope constraints. *Econ. Geol. Bull. Soc.* **2001**, *96*, 583–598. [CrossRef]

29. Tian, J.X.; Ren, Z.L.; Song, Z.Y.; Huang, S.Q.; Li, S.Z.; Zhang, H.; Xie, Y.J.; Zhang, Y.F. *Report on Geological Survey of Diyanqinamu Molybdenum-Silver Polymetallic Deposit in Dong, Ujimqin Banner, Inner Mongolia*; The First Geological Exploration Institute of General Administration of Metallurgical Geology of China: Sanhe City, China, 2012; Unpublished work. (in Chinese)

30. Yan, H.; Huang, F.X.; Sun, H.; Zhao, L.Q.; Zhang, Y.; Zhang, H.; Li, S.Z.; Liu, F.F.; Wang, J.S. A Model for Alteration Zoning of Hydrothermal Mineralization Based on Surpae Software for the Diyanqinamu Mo Mine District, Inner Mongolia. *Geol. Prospect.* **2012**, *48*, 932–939. (in Chinese with English abstract)

31. Shao, J.A.; Zhang, Q.; Mu, B.L. Distribution of Uranium and Molybdenum Deposits and Their Relations with Medium Massifs in Central Asian Orogenic Zone. *J. Jilin Univ. Earth Sci. Ed.* **2011**, *41*, 1667–1675. (in Chinese with English abstract)

32. Sun, H.R.; Huang, Z.L.; Li, W.B.; Leng, C.B.; Ma, D.Y.; Zhang, X.C. Chronology, geochemistry and Sr-Nd isotope studies of Jurassic intrusions in the Diyanqinamu porphyry Mo mine, central Inner Mongolia, China. *J. Asian Earth Sci.* **2014**, *88*, 85–97. [CrossRef]

33. Wu, F.Y.; Sun, D.Y.; Ge, W.C.; Zhang, Y.B.; Grant, M.L.; Wilde, S.A.; Jahn, B.M. Geochronology of the Phanerozoic granitoids in northeastern China. *J. Asian Earth Sci.* **2011**, *41*, 1–30. [CrossRef]

34. Jahn, B.M.; Capdevila, R.; Liu, D.Y.; Vernon, A.; Badarch, G. Sources of Phanerozoic granitoids in the transect Bayanhongor–Ulaan Baatar, Mongolia: Geochemical and Nd isotopic evidence, and implications for Phanerozoic crustal growth. *J. Asian Earth Sci.* **2004**, *23*, 629–653. [CrossRef]

35. Chen, Y.J.; Chen, H.Y.; Zaw, K.; Pirajno, F.; Zhang, Z.J. Geodynamic settings and tectonic model of skarn gold deposits in China: An overview. *Ore Geol. Rev.* **2007**, *31*, 139–169. [CrossRef]

36. Meng, Q.R. What drove late Mesozoic extension of the northern China-Mongolia tract? *Tectonophysics* **2003**, *369*, 20. [CrossRef]

37. Xu, W.L.; Pei, F.P.; Wang, F.; Meng, E.; Ji, W.Q.; Yang, D.B.; Wang, W. Spatial-temporal relationships of Mesozoic volcanic rocks in NE China: Constraints on tectonic overprinting and transformations between multiple tectonic regimes. *J. Asian Earth Sci.* **2013**, *74*, 167–193. [CrossRef]

38. Ying, J.F.; Zhou, X.H.; Zhang, L.C.; Wang, F. Geochronological framework of Mesozoic volcanic rocks in the Great Xing'an Range, NE China, and their geodynamic implications. *J. Asian Earth Sci.* **2010**, *39*, 786–793. [CrossRef]

39. Zhang, J.H.; Gao, S.; Ge, W.C.; Wu, F.Y.; Yang, J.H.; Wilde, S.A.; Li, M. Geochronology of the Mesozoic volcanic rocks in the Great Xing'an Range, northeastern China: Implications for subduction-induced delamination. *Chem. Geol.* **2010**, *276*, 144–165. [CrossRef]

40. Zhang, F.Q.; Chen, H.L.; Yu, X.; Dong, C.W.; Yang, S.F.; Pang, Y.M.; Batt, G.E. Early Cretaceous volcanism in the northern Songliao Basin, NE China, and its geodynamic implication. *Gondwana Res.* **2011**, *19*, 163–176. [CrossRef]

41. Mao, J.W.; Xie, G.Q.; Zhang, Z.H.; Li, X.F.; Wang, Y.T.; Zhang, C.Q.; Li, Y.F. Mesozoic large-scale metallogenic pulses in North China and corresponding geodynamic settings. *Acta Pet. Sin.* **2005**, *21*, 169–188. (in Chinese with English abstract)

42. Hong, D.W.; Wang, S.; Xie, G.L.; Zhang, J.S. Genesis positive ε(Nd,t) grantoids in the Da Hinggan Mts.-Mongolia Orogenic belt and growth continental crust. *Earth Sci. Front.* **2000**, *7*, 441–456. (in Chinese with English abstract)

43. Wu, F.Y.; Sun, D.Y.; Li, H.M.; Jahn, B.M.; Wilde, S. A-type granites in northeastern China: Age and geochemical constraints on their petrogenesis. *Chem. Geol.* **2002**, *187*, 143–173. [CrossRef]

44. Zeng, Q.D.; Liu, J.M.; Yu, C.M.; Ye, J.; Liu, H.T. Metal deposits in the Da Hinggan Mountains, NE China: Styles, characteristics, and exploration potential. *Int. Geol. Rev.* **2011**, *53*, 846–878. [CrossRef]

45. Xue, H.M.; Guo, L.J.; Hou, Z.Q.; Zhou, X.W.; Tong, Y.; Pan, X.F. The Xilingele complex from the eastern part of the Central Asian-Mongolia Orogenic Belt, China: Products of Early Variscan orogeny other than ancient block: Evidence from zircon SHRIMP U-Pb ages. *Acta Pet. Sin.* **2009**, *25*, 2001–2010. (in Chinese with English abstract)

46. Nie, F.J.; Jiang, S.H.; Zhang, Y.; Bai, D.M.; Hu, P.; Zhao, Y.Y.; Zhang, W.Y.; Liu, Y. *Metallogenic Studies and Prospecting Orientation in Central and Eastern Segments Along China-Mongolia Border*; Geologic Publishing House: Beijing, China, 2007. (in Chinese with English abstract)

47. Hong, D.W.; Wang, S.G.; Xie, X.L.; Zhang, J.S.; Wang, T. Metallogenic province derived from mantle sources: Nd, Sr, S and Pb isotope evidence from the Central Asian Orogenic Belt. *Gondwana Res.* **2003**, *6*, 711–728.

48. Ge, W.C.; Wu, F.Y.; Zhou, C.Y.; Zhang, J.H. Porphyry Cu-Mo deposits in the eastern Xing'an-Mongolian Orogenic Belt: Mineralization ages and their geodynamic implications. *Chin. Sci. Bull.* **2007**, *52*, 3416–3427. (in Chinese with English abstract) [CrossRef]

49. Zhang, W.Y.; Nie, F.J.; Jiang, S.H.; Liu, Y.; Hu, P.; Xu, D.Q.; Cui, X.M.; Bai, D.M. *Magmatic Activity and Metallogeny of Dong Ujimqin Banner, Inner Mongolia*; Geological Publishing House: Beijing, China, 2009. (in Chinese with English abstract)

50. Sun, H.R.; Huang, Z.L.; Yan, Z.F.; Yan, G.S.; Lv, Z.C. Geochemical Characteristics and Geological Significance of 260 Ma Basalt from Inner Mongolia, China. *Acta Mineral. Sin.* **2015**, *35*, 529–539.

51. Nie, F.J.; Hu, P.; Jiang, S.H.; Liu, Y.F. Geological Features, Geochronology and Origin of the Tungsten and Tungsten(Molybdenum)Deposits in the Shamai-Yuguzer Mineralization Concentrated Camp along the Sino-Mongolian Border. *Acta Geosci. Sin.* **2010**, *31*, 383–394. (in Chinese with English abstract)

52. Wang, R.; Zhang, Z.C.; Zeng, Q.D.; Wang, Y.B.; Guo, Q.; Chu, H.Y.; Guo, Y.P.; Guo, L.X. The characteristics of ore-forming Fluids and ore-forming mechanism of the Diyanqinamu super-large molybdenum deposit, Inner Mongolia. *Acta Pet. Sin.* **2018**, *34*, 3582–3596. (in Chinese with English abstract)

53. Barton, P.B., Jr.; Bethke, P.M. Chalcopyrite disease in sphalerite: Pathology and epidemiology. *Am. Miner.* **1987**, *72*, 451–467.

54. Belshaw, N.S.; Freedman, P.A.; O'Nions, R.K.; Frank, M.; Guo, Y. A new variable dispersion double-focusing plasma mass spectrometer with performance illustrated for Pb isotopes. *Int. J. Mass Spectrom.* **1998**, *181*, 51–58. [CrossRef]

55. Ohmoto, H. Systematics of Sulfur and Carbon Isotopes in Hydrothermal Ore Deposits. *Econ. Geol.* **1972**, *67*, 551–578. [CrossRef]

56. Zartman, R.E.; Doe, B.R. Plumbotectonics—The Model. *Tectonophysics* **1981**, *75*, 135–162. [CrossRef]

57. Dixon, G.; Davidson, G.J. Stable isotope evidence for thermochemical sulfate reduction in the Dugald river (Australia) strata-bound shale-hosted zinc-lead deposit. *Chem. Geol.* **1996**, *129*, 227–246. [CrossRef]

58. Ohmoto, H.; Kaiser, C.J.; Geer, K.A. Systematics of Sulphur Isotopes in Recent Marine Sediments and Ancient Sediment-Hosted Base Metal Deposits. In *Stable Isotopes and Fluid Processes in Mineralization 23*; Herbert, H.K., Ho, S.E., Eds.; University of Western Australia: Crawley, Australia, 1990.

59. Baoyin, W.L.J.; Liu, H.M.; Zhao, Z.Y.; He, H.Y.; Hao, X.L.; Wang, Z.Y. Geologic chracteristics and prospecting potentiality of the Pb-Zn polymetal deposits in Huahalejin area, Inner Mongolia. *Geol. Resour.* **2012**, *21*, 432–436. (in Chinese with English abstract)

60. Sillitoe, R.H. The tops and bottoms of porphyry copper deposits. *Econ. Geol.* **1973**, *68*, 799–815. [CrossRef]

61. Kong, W.Q.; Liu, C.; Deng, J.F.; Xu, L.Q.; Tao, J.X.; Luo, Z.H.; Zhao, G.C. The characteristics of igneous rock and LA-ICP MS zircon dating in Wuhuaaobao Mo deposit, Erlianhot area of Inner Mongolia. *Earth Sci. Front.* **2012**, *19*, 123–135. (in Chinese with English abstract)